Acta Crystallographica Section D
Biological Crystallography
ISSN 0907-4449

Adenosine kinase from *Schistosoma mansoni*: structural basis for the differential incorporation of nucleoside analogues

Larissa Romanello,[a] José Fernando Ruguiero Bachega,[a] Alexandre Cassago,[b] José Brandão-Neto,[c] Ricardo DeMarco,[a] Richard Charles Garratt[a] and Humberto D'Muniz Pereira[a]*

[a]Centro de Biotecnologia Molecular Estrutural, Instituto de Física de São Carlos, Universidade de São Paulo, Avenida Trabalhador Saocarlense 400, São Carlos-SP 13566-590, Brazil, [b]Laboratório Nacional de Biociências – LNBIO, CP 6192, Campinas-SP 13083-970, Brazil, and [c]Diamond Light Source, Harwell Science and Innovation Campus, Didcot, Oxfordshire OX11 0DE, England

Correspondence e-mail: hmuniz.pereira@gmail.com

Received 11 July 2012
Accepted 29 October 2012

PDB References: SmAK–adenosine, 3vas; 3vaq; SmAK–Ado–AMP, 3uq6; SmAK–tubercidin, 3uq9; SmAK–2-fluoroadenosine, 4dc3

In adult schistosomes, the enzyme adenosine kinase (AK) is responsible for the incorporation of some adenosine analogues, such as 2-fluoroadenosine and tubercidin, into the nucleotide pool, but not others. In the present study, the structures of four complexes of *Schistosoma mansoni* AK bound to adenosine and adenosine analogues are reported which shed light on this observation. Two differences in the adenosine-binding site in comparison with the human counterpart (I38Q and T36A) are responsible for their differential specificities towards adenosine analogues, in which the *Schistosoma* enzyme does not tolerate bulky substituents at the N7 base position. This aids in explaining experimental data which were reported in the literature more than two decades ago. Furthermore, there appears to be considerable plasticity within the substrate-binding sites that affects the side-chain conformation of Ile38 and causes a previously unobserved flexibility within the loop comprising residues 286–299. These results reveal that the latter can be sterically occluded in the absence of ATP. Overall, these results contribute to the body of knowledge concerning the enzymes of the purine salvage pathway in this important human parasite.

1. Introduction

Schistosoma mansoni is one of the parasitic species responsible for the disease schistosomiasis; in 2005, the World Health Organization estimated that approximately 200 million people were infected with it (World Health Organization, 2005). It is known that schistosomes (Senft, Crabtree *et al.*, 1973; Senft, Senft *et al.*, 1973) and schistosomules (Dovey *et al.*, 1984) are unable to synthesize purine bases *de novo* and therefore the purine-salvage pathway is exclusively used to supply purine bases for energy requirements and nucleic acid synthesis. This pathway was elucidated in schistosomes and schistosomules in the 1970s and 1980s by the work of Senft (Miech *et al.*, 1975; Senft & Crabtree, 1977, 1983; Senft, Crabtree *et al.*, 1973; Senft *et al.*, 1972; Senft, Senft *et al.*, 1973; Stegman *et al.*, 1973; Crabtree & Senft, 1974) and Dovey (Dovey *et al.*, 1984).

Schistosomes can incorporate adenine, adenosine, inosine and hypoxanthine into ATP. Adenine is anabolized to AMP *via* adenine phosphoribosyltransferase (APRT). Adenosine can be incorporated *via* two different mechanisms: the adenosine kinase reaction, yielding AMP, and the indirect pathway (adenosine → inosine → hypoxanthine → IMP → AMP), which requires the enzymes adenosine deaminase (ADA), purine nucleoside phosphorylase (PNP), hypoxanthine-guanine phosphoribosyltransferase (HGPRT), adenylosuccinate synthase (ADSS) and adenylosuccinate

lyase (ADSL). Interestingly, the indirect pathway is much more active in schistosomes than that directly employing adenosine kinase (Stegman *et al.*, 1973). These same authors related that the nucleoside analogues tubercidin and 2-fluoroadenosine are not deaminated by ADA and are also not substrates of PNP. They concluded that these analogues must be converted to the corresponding 5′-monophosphate nucleotides by the adenosine kinase enzyme.

Adenosine kinase activity was first identified in cell-free extracts of schistosomes using ^{14}C-methyl-labelled 6-mercaptopurine ribonucleoside and adenosine-8-^{14}C as substrates (Senft, Senft *et al.*, 1973). When the latter was used as a substrate, significant amounts of labelled AMP and IMP were found, indicating that schistosomes have multiple mechanisms for incorporating preformed purine bases and nucleosides into the purine-nucleotide pool. It was estimated that the APRT activity is ten times greater than the adenosine kinase activity, which in turn is greater than that of HGPRT (Senft, Senft *et al.*, 1973). It was concluded that the adenosine kinase pathway accounts for about 30% of the total conversion of adenosine into AMP. Furthermore, similar studies minimized the significance of the adenosine kinase reaction (Crabtree & Senft, 1974; Senft, Crabtree *et al.*, 1973; Senft, Senft *et al.*, 1973). On the other hand, when coformycin, an extremely potent inhibitor of adenosine deaminase, was used the anabolism of adenosine in intact *S. mansoni in vitro* was not inhibited (Senft & Crabtree, 1977), but rather was significantly stimulated. The inhibition of ADA increases the level of adenosine, which becomes available for the alternative pathways (the AK and AP–APRT pathways).

Adenosine kinase (EC 2.7.1.20) catalyses the phosphorylation of adenosine using ATP as the phosphoryl donor in the presence of magnesium, generating AMP and ADP (Carret *et al.*, 1999). Adenosine kinase belongs to the ribokinase family, with which it shares common structural features based on a central eight-stranded β-sheet flanked by eight conserved α-helices. The active site lies in a shallow groove along the edge of the β-sheet, with the phosphate-acceptor hydroxyl group and γ-phosphate of ATP close together towards the centre of the groove and the main substrate and ATP-binding sites at the ends (Zhang *et al.*, 2004).

Adenosine kinase shows a relatively broad substrate specificity, tolerating modifications to both the sugar and base moieties (Miller *et al.*, 1979); numerous nucleoside antiviral and anticancer drugs are AK substrates and consequently undergo rapid phosphorylation *in vivo* to their 5′-monophosphate derivatives (Mathews *et al.*, 1998). Several purine analogues have been used in the past in the experimental treatment of schistosomiasis (Dovey *et al.*, 1985; el Kouni *et al.*, 1987; el Kouni, 1991). el Kouni & Cha (1987) investigated the incorporation of nine adenosine analogues (5′-deoxy-5′-iodo-2-fluoroadenosine, tubercidin, nebularine, toyocamycin, sangivamycin, 3′-deoxysangivamycin, 9-deazaadenosine, 7,9-dideaza-7-thiaadenosine and 1-methyformicin) into intact adult worms, demonstrating that *S. mansoni* could incorporate six of these compounds into the nucleoside pool, with the exceptions being sangivamycin, 3′-deoxysangivamycin and 1-methylformicin. All of the analogues only entered the nucleotide pool after phosphorylation by adenosine kinase, demonstrating the importance of adenosine kinase in the metabolism of various adenosine analogues by the parasite. The same authors suggested that the metabolism of these analogues in *S. mansoni* follows the same pathways as are observed in mammals, being phosphorylated by adenosine kinase to their respective 5′-monophosphates and then on to nucleotide diphosphates and triphosphates (el Kouni & Cha, 1987).

In the present article, we describe the cloning, expression, purification, crystallization and structure determination of *S. mansoni* adenosine kinase (SmAK) in the form of four different complexes: SmAK–adenosine–AMP, SmAK–adenosine, SmAK–tubercidin and SmAK–2-fluoroadenosine. These structures help to explain the AK selectivity reported in the 1980s by El Kouni and Cha for SmAK when compared with the human enzyme. This is only the third structure of an enzyme from the *S. mansoni* salvage pathway to be reported to date and adds to our body of knowledge concerning purine metabolism in this important human parasite.

2. Materials and methods

2.1. Cloning, expression and purification of adenosine kinase

The coding sequence for adenosine kinase was obtained by searching the *S. mansoni* genome project database (http://www.genedb.org/Homepage/Smansoni; code Smp_008360). Forward (5′-ACTGTATGCTAGCATGCACGATTTATCG-3′) and reverse (5′-TACAGTCTCGAGCTATTTGTTTATT-TTTAAGG-3′) primers were designed in order to amplify the AK gene, adding restriction sites (*Nhe*I and *Xho*I) for subcloning into the expression vector pET28a.

cDNA was obtained by RT-PCR employing the SuperScript III First-Strand Synthesis System from Promega. The RT product was used as a template for PCR using *Taq* DNA polymerase from Fermentas and the following cycling parameters: 3 min denaturation at 369 K, 35 cycles of 30 s at 369 K, 1 min at 325.5 K, 1.5 min at 345 K and a final 10 min elongation at 345 K. An amplification product of about 1000 bp was recovered from a 1% agarose gel; after adenylation, it was cloned into the pGEM cloning vector (Promega) and transformed into *Escherichia coli* DH5α cells. Transformants were selected using the chromogenic substrate X-gal and by colony PCR. The AK2 gene was then digested with *Nhe*I and *Xho*I (New England Biolabs) and recovered on a 1% agarose gel. pET28a was digested using the same enzymes and the pET28a-AK construct was synthesized by treatment with T4 DNA ligase (New England Biolabs) overnight at 277 K. *E. coli* DH5α cells transformed with this plasmid were selected on LB agar plates containing kanamycin (50 mg ml^{-1}). The pET28a-AK product obtained from the *E. coli* transformants was confirmed by colony PCR and used to transform *E. coli* BL21 (DE3) cells. The AK gene sequence of pET28a-AK was confirmed by sequencing.

Table 1
Full data-collection and refinement statistics.

Values in parentheses are for the highest shell.

	Adenosine–AMP	Tubercidin	Adenosine, occluded loop	Adenosine, open loop	2-Fluoroadenosine
Data collection					
Space group	$P2_12_12$	$P2_12_12$	$P2_12_12$	$P2_12_12$	$P2_12_12$
Unit-cell parameters					
a (Å)	58.99	59.56	58.97	59.10	59.35
b (Å)	180.53	181.51	180.12	180.31	179.39
c (Å)	78.32	78.55	79.27	79.43	79.74
Detector	MAR Mosaic 225	R-AXIS IV^{++}	Quantum 315	Quantum 315	Quantum 315
X-ray source	LNLS MX2	Rigaku MicroMax-007	Diamond I04	Diamond I04	Diamond I04
Wavelength (Å)	1.45	1.54	0.961	0.961	0.961
Resolution range (Å)	49.96–2.30 (2.42–2.30)	20.0–2.35 (2.48–2.35)	90.06–2.26 (2.32–2.26)	79.43–2.46 (2.52–2.44)	56.35–2.40 (2.53–2.40)
Multiplicity	3.4 (3.4)	2.7 (2.2)	3.9 (3.9)	3.9 (3.4)	4.3 (4.3)
$R_{\rm meas}$† (%)	12.1 (64.5)	8.8 (45.1)	13.3 (75.6)	12.1 (89.7)	12.0 (66.2)
Completeness (%)	93.3 (88.6)	96.6 (88.2)	97.9 (97.9)	99.6 (99.2)	91.4 (94.2)
Total reflections	123531 (16846)	95546 (11340)	156492 (11092)	121563 (8523)	134423 (19833)
Unique reflections	35825 (4886)	35262 (5056)	40097 (5453)	31568 (2280)	30923 (4588)
$\langle I/\sigma(I)\rangle$	10.7 (2.1)	11.82 (2.38)	6.43 (1.63)	10.5 (1.9)	8.7 (2.9)
Refinement parameters					
Reflections used for refinement	35871	35239	40097	32317	30864
R‡ (%)	20.8	17.3	17.7	18.73	18.94
$R_{\rm free}$ (%)	23.0	22.7	22.9	23.01	22.85
No. of protein atoms	5242	5305	5352	5374	5328
No. of ligand atoms	86	58	40	40	40
B (Å^2)					
Protein	43.48	32.53	36.08	51.52	40.13
Ligands	44.30	30.64	21.51	37.12	23.22
Waters	42.00	38.51	33.49	48.50	39.75
Cruickshank DPI (Å)	0.21	0.21	0.23	0.19	0.24
Ramachandran plot					
Favoured (%)	97.61	97.63	98.24	97.81	97.78
Allowed (%)	2.39	2.37	1.76	2.19	2.22
Outliers (%)	0.0	0.0	0.0	0.0	0.0
All-atom clashscore	7.03	5.93	5.79	5.76	6.84
R.m.s.d. from ideal geometry					
Bond lengths (Å)	0.002	0.003	0.004	0.002	0.002
Bond angles (°)	0.575	0.778	0.819	0.574	0.544
PDB code	3uq6	3uq9	3vaq	3vas	4dc3

† $R_{\rm meas} = \sum_{hkl}\{N(hkl)/[N(hkl)-1]\}^{1/2}\sum_i |I_i(hkl) - \langle I(hkl)\rangle|/\sum_{hkl}\sum_i I_i(hkl)$. ‡ $R = \sum_{hkl}\big||F_{\rm obs}| - |F_{\rm calc}|\big|/\sum_{hkl}|F_{\rm obs}|$.

The preculture was shaken overnight at 310 K, inoculated into culture at a ratio of 1:100 and grown to an OD_{600} of 0.6. Expression was induced by the addition of 0.1 m*M* IPTG and allowed to proceed for 3 h at 310 K. The cells were centrifuged at 9000*g* for 20 min at 277 K, suspended in lysis buffer (50 m*M* sodium phosphate pH 7.8, 300 m*M* NaCl, 10 m*M* imidazole, 5 m*M* β-mercaptoethanol, 1 m*M* $MgCl_2$) and cooled to 253 K overnight. The cells were lysed using a 6 min sonication and centrifuged at 10 000*g* for 20 min at 277 K, and the AK2 in the soluble fraction was purified on an Ni–NTA agarose column (Qiagen) equilibrated with ten column volumes of lysis buffer, washed with ten column volumes of wash buffer (50 m*M* sodium phosphate pH 7.8, 300 m*M* NaCl, 20 m*M* imidazole, 5 m*M* β-mercaptoethanol, 1 mM $MgCl_2$) and eluted with six column volumes of elution buffer (50 m*M* sodium phosphate pH 7.8, 300 m*M* NaCl, 200 m*M* imidazole, 5 m*M* β-mercaptoethanol, 1 m*M* $MgCl_2$). Fractions of the purifications were visualized using SDS–PAGE. A second purification step was carried out with AMP–agarose affinity resin (Sigma–Aldrich). The column was equilibrated with ten volumes of 50 m*M* sodium phosphate pH 7.8, 200 m*M* NaCl, 5 m*M* β-mercaptoethanol, 1 m*M* $MgCl_2$ and the fractions containing AK2 from the previous purification were applied. The column was washed and the AK2 was eluted using the same buffer including 2 m*M* AMP. Fractions were visualized using SDS–PAGE.

2.2. Crystallization and data collection

The purified SmAK2 was dialyzed against 20 m*M* Tris pH 7.8, 200 m*M* NaCl, 5 m*M* β-mercaptoethanol, 1 m*M* $MgCl_2$, 2 m*M* AMP and concentrated to 4 mg ml^{-1}. The protein was subjected to robotic crystallization trials with a Honeybee 963 robot (Genomic Solutions) using the crystallization kits SaltRX, Index HT (Hampton Research), The PEGs Suite and The Classics Suite (Qiagen) in Greiner CrystalQuick sitting-drop plates employing 1 µl AK2 solution and 1 µl well solution. The plates were incubated at 291 K. AK2 crystals were obtained after one week in condition G3 of Index HT, which consists of 100 m*M* bis-Tris pH 6.5, 200 m*M* Li_2SO_4, 25% PEG 3350. Manual optimization was performed by varying the PEG 3350 concentration (from 21% to 27%) and by using five different pH values (6.1, 6.3, 6.5, 6.7 and 6.9) in bis-Tris buffer. The crystals were transferred into a cryoprotective solution

(mother liquor plus 20% glycerol), mounted in cryoloops and cooled directly in liquid nitrogen for data collection. This structure proved to be a complex of SmAK containing both adenosine and AMP and will henceforth be referred to as SmAK–Ado–AMP. Enzyme prepared under identical conditions was also dialyzed exhaustively in the same buffer lacking AMP and adenosine in an attempt to obtain an apo structure. These crystals were also rapidly cooled for data collection. However, despite the dialysis procedure, the resulting structure turned out to be that of a complex with adenosine alone and will be referred to here as SmAK–adenosine. Complexes with tubercidin (SmAK–tubercidin) and with 2-fluoroadenosine (SmAK–fluoradenosine) were obtained by cocrystallization of the enzyme in the presence of 2 m*M* ligand under the crystallization conditions described above.

X-ray diffraction data were collected at 100 K on beamline MX2 of the LNLS (Campinas, Brazil; SmAK–Ado–AMP), on a home source (Rigaku MicroMax-007 equipped with an R-AXIS IV^{++} detector; SmAK–tubercidin) or on beamline I04 of the Diamond Light Source (SmAK–adenosine, SmAK–tubercidin and SmAK–fluoroadenosine). The data were indexed, integrated and scaled using the programs *iMOSFLM* (Battye *et al.*, 2011) and *SCALA* from the *CCP*4 suite (Winn *et al.*, 2011) in the cases of the SmAK–AMP–adenosine and SmAK–fluoroadenosine complexes, using the *XDS* package (Kabsch, 2010) for SmAK–tubercidin and using *xia*2 for SmAK2–adenosine. All of the crystals diffracted to resolutions within the range 2.26–2.4 Å (Table 1).

2.3. Structure resolution and refinement

The first structure to be solved was the AK2–AMP–adenosine complex obtained by cocrystallization. This structure was solved by molecular replacement with the program *Phaser* (McCoy, 2007) using human adenosine kinase (PDB entry 1bx4; Mathews *et al.*, 1998) as the search model after modification using the *CHAINSAW* program (Stein, 2008). Human AK shares 33% sequence identity with its *Schistosoma* homologue. The Matthews coefficient indicated the presence of two molecules in the asymmetric unit, which were readily located by molecular replacement and related by noncrystallographic symmetry. Structure refinement was carried out using *PHENIX* (Adams *et al.*, 2002) and *Coot* for model building (Emsley *et al.*, 2010) using σ_A-weighted $2F_o - F_c$ and $F_o - F_c$ electron-density maps. The ligands were automatically placed using the Find Ligand routine of *Coot*, and water molecules were located using a combination of *Coot* and *PHENIX*.

The structure of the SmAK–tubercidin complex was also solved by molecular replacement, this time employing the previously solved structure of SmAK–Ado–AMP as the search model. Subsequently, the SmAK–adenosine complex was solved using the refined SmAK–tubercidin structure; finally, the structure of the SmAK–2-fluoroadenosine complex was similarly solved employing the SmAK–adenosine structure. In all cases, a similar refinement protocol to that described above for SmAK–Ado–AMP was employed.

In all cases, the behaviour of R and R_{free} was used as the principal criterion for validating the refinement protocol and the stereochemical quality of the model was evaluated with *PROCHECK* (Lazarowski *et al.*, 1997) and *MolProbity* (Chen *et al.*, 2010). The data-collection and processing parameters are given in Table 1. The coordinates and structure factors have been deposited in the PDB with the following codes: 3vas and 3vaq for SmAK–adenosine, 3uq6 for SmAK–Ado–AMP, 3uq9 for SmAK–tubercidin and 4dc3 for SmAK–2-fluoroadenosine. The data-processing and refinement statistics are also given in Table 1.

2.4. Small-molecule preparation, molecular docking and molecular modelling

In order to investigate the structural basis for the differential incorporation of adenosine analogues observed by el Kouni & Cha (1987), the structure of ten known bioactive ligands of the *Schistosoma* and human adenosine kinase enzymes [adenosine, 1-methylformycin, tubercidin (7-deazaadenosine), nebularine, 7,9-dideaza-7-thioadenosine, 5′-deoxy-5-iodo-2-fluoradenosine, sangivamycin, 9-deazaadenosine, 3-deoxysangivamycin and toyocamycin] were built with *Avogadro*. All of the structures generated were minimized with the MMFF94s force field available in *Avogadro*.

Molecular docking of adenosine analogous to that in the structures of the human (HuAK; Mathews *et al.*, 1998) and *S. mansoni* (SmAK2) enzymes was carried out using *Autodock Vina* 1.0 (Trott & Olson, 2010) through the available *PyMOL* interface (Seeliger & de Groot, 2010). The polar H atoms and charge distributions were assigned using *Autodock Tools* 1.5.4. The default grid spacing of 0.372 Å was used with a box of $50 \times 50 \times 50$ points centred on the adenosine-binding site. For SmAK, resides Ile38, Met134 and Thr136 were selected as flexible during docking.

2.5. Activity and kinetics analysis

The determination of the enzyme specific activity for adenosine, 2-fluoroadenosine and tubercidin was measured by coupling the production of ADP to NADH reduction using a lactate dehydrogenase/pyruvate kinase coupled assay (Datta *et al.*, 1987), which could be followed spectrophotometrically at 340 nm. Assays (in octuplicate) were carried out using a SpectraMax Plus384 instrument with a 200 µl reaction volume in a 96-well plate format using 100 m*M* Tris–HCl pH 7.4, 200 m*M* NaCl, 5 m*M* $MgCl_2$, 1 m*M* phosphoenolpyruvate, 0.1 m*M* NADH, 5 U ml^{-1} LDH and PK, 1 m*M* ATP, 84.2 n*M* SmAK and 50 µ*M* nucleoside or nucleoside analogue. The determination of the kinetic constants for the second substrate, ATP, was performed as described above using variable amounts of ATP (ten data points from 500 to 13 µ*M* ATP in 1:1.5 serial dilutions). The reaction was started by the addition of 84 n*M* SmAK and was monitored in a microplate reader at 340 nm for up to 8 min. All measurements were made in triplicate. Kinetic parameters were estimated by nonlinear regression using the *GraphPad Prism* software.

3. Results and discussion

3.1. Expression, purification and crystal structure determination

The sequence of the SmAK gene codes for a protein of 352 residues with a calculated molecular mass of 39 392.5 Da. Sequence analysis reveals that SmAK shares the following levels of sequence identity with other AKs: human, 38%; *Anopheles gambiae*, 35%; *Trypanosoma brucei*, 31%; *Toxoplasma gondii*, 23%; *Sinorhizobium meliloti*, 23% (Fig. 1). No significant sequence identity was found with *Mycobacterium tuberculosis* AK.

Heterologous expression of SmAK yielded approximately 4 mg per litre of medium, and the use of an AMP-agarose column as the second step in purification proved to be essential for its purification. Gel-filtration analysis showed SmAK to be monomeric, which is in agreement with expectation based on the human and *T. gondii* homologues (data not shown).

SmAK was crystallized using 100 m*M* bis-Tris pH 6.1–6.7, 200 m*M* lithium sulfate, 21–27% PEG 3350. Crystals appeared after one week and grew to a maximum of 0.4 mm in their largest dimension. They were very heterogeneous in diffraction quality and it was necessary to screen about 10–20 crystals in all cases in order to obtain one that diffracted to sufficient resolution (around 2.3 Å). It proved not to be possible to obtain an apo structure, even when SmAK was exhaustively dialyzed in buffer in the absence of both AMP and adenosine.

SmAK crystallized in the orthorhombic space group $P2_12_12$ with two molecules in the asymmetric unit, and the first structure (the SmAK–adenosine–AMP complex) was readily solved by molecular replacement using human AK (PDB entry 1bx4) as a search model. Five complexes of *S. mansoni* adenosine kinase are reported here: two with adenosine alone, one bound simultaneously to adenosine and AMP, and one each of the complexes with tubercidin and 2-fluoroadenosine. This is the first time that complexes of tubercidin and 2-fluoroadenosine with a monomeric AK have been described.

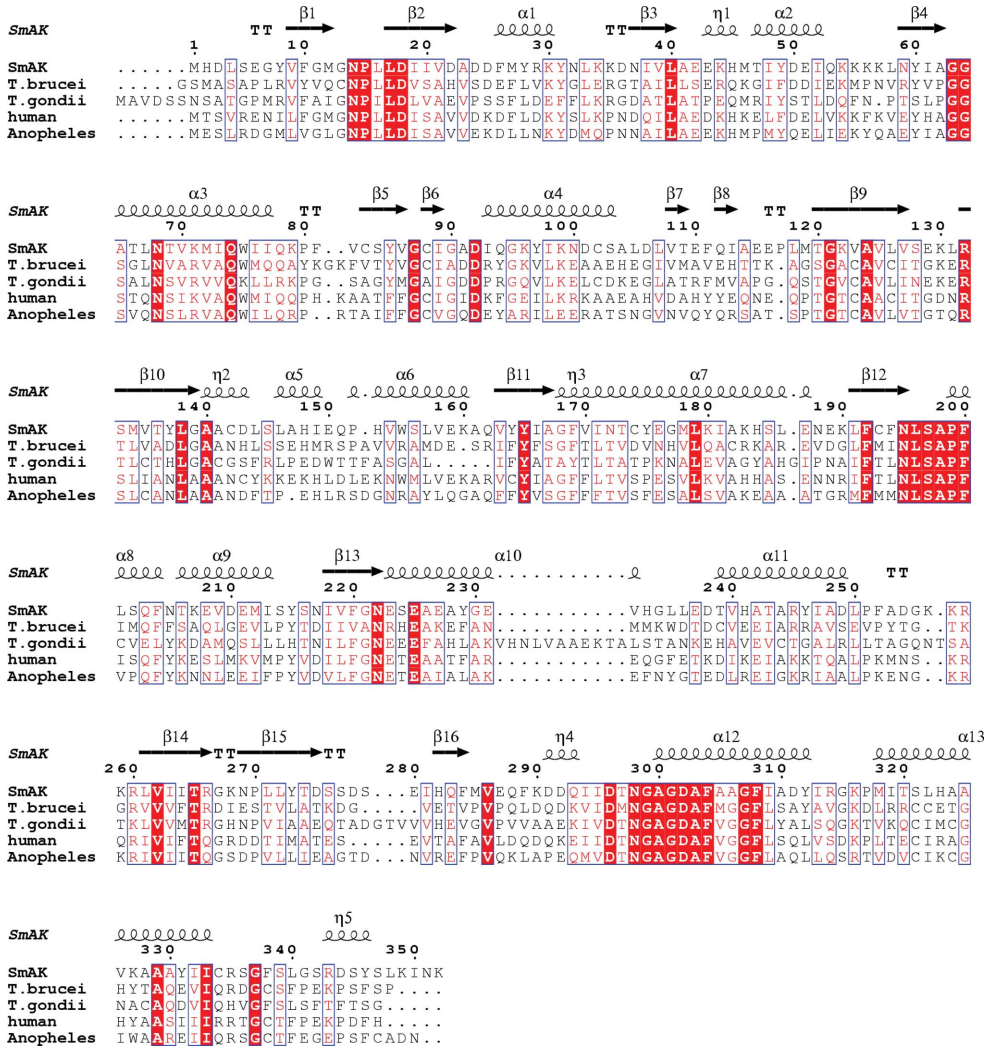

Figure 1
Alignment of AKs from *Schistosoma mansoni*, *Trypanosoma brucei*, *Toxoplasma gondii*, *Homo sapiens* and *Anopheles gambiae*.

The overall structure is similar to that previously reported for human adenosine kinase (Mathews *et al.*, 1998), as well as those from *T. gondii* (Schumacher *et al.*, 2000; Cook *et al.*, 2000), *A. gambiae* (Cassera *et al.*, 2011), *T. brucei* (Kuettel *et al.*, 2011) and *S. meliloti* (PDB entry 3ubo; New York Structural Genomics Research Consortium, unpublished work), and consists of two domains, the large domain and the lid domain, containing a total of 15 β-strands, 15 α-helices and three 3_{10}-helices. The lid domain possesses a sheet with topology 3, −4X, 2, 1 and is formed by noncontiguous β-strand elements plus two α-helices ($\beta2$–$\alpha1$–$\beta3$–$\alpha2$–$\beta4$–$\beta8$–$\beta9$). The large domain is composed of an α/β structure with a 1X, 1X,−2X, −1X, −1X, −1X, −1, −1 β-sheet topology as determined by *PROMOTIF* (Hutchinson & Thornton, 1996). The β-structure is formed by strands $\beta1$, $\beta5$–$\beta7$ and $\beta10$–$\beta15$ surrounded by the α-helical elements $\alpha3$–$\alpha13$. The lateral side of the final strand is exposed to the solvent and is composed of polar residues, with the exception of Met285.

Some residues could not be observed in the electron-density maps and were removed from the

final models; these residues mainly lie at the N- and C-termini and in residues 129–132 of some subunits.

Superposition of all ten SmAK structures results in r.m.s.d. values which vary between 0.17 and 0.75 Å, with the largest deviation being observed for the two adenosine complexes. As expected, larger deviations were observed in the lid domain, but these were not as large as those observed on comparing the previously described open and closed conformations (Cassera *et al.*, 2011). As such, all of the SmAK structures described here can be considered to be in the lid-closed conformation when compared with other homologues. Nevertheless, our structures can be readily grouped into two clusters with respect to the conformation of the lid domain; specifically, the loop from residues 288 to 299 and the β-turn between residues 128 and 131. These two conformations correspond to the two different molecules of the asymmetric unit and appear to be related to the observed differences in accessibility to the active site as demonstrated in the 2-fluoroadenosine complex, in which the ligand is bound to only one molecule. Indeed, the conformation of the 288–299 loop in this molecule is similar to that observed for the complex with two tubercidin molecules in SmAK–tubercidin, clearly indicating two different conformations in the asymmetric unit. In the molecules in which the 288–299 loop is well ordered it enters the ATP-binding site and results in its occlusion, the consequences of which are described below.

3.2. Active-site description

3.2.1. Adenosine-binding site. The adenosine-binding site (ABS) was characterized by using information from all five of the complexes described here. In all cases the ABS is occupied either by adenosine or by an adenosine analogue (tubercidin or 2-fluoroadenosine). In the case of the complex with adenosine alone, the ligand was not added during sample preparation and was therefore presumably acquired from the bacteria during heterologous expression. All attempts to obtain an apo structure using dialysis were unsuccessful. In the following description we will use molecule *A* of the SmAK–Ado–AMP complex as a template unless stated otherwise. As in other AKs, the active site is located along the C-terminal edge of the central β-sheet of the large domain, in which the ABS is located near to the lid domain and the ATP-binding site is found at the opposite end (Zhang *et al.*, 2006). In all structures reported here, clear electron density was visible in the ABS compatible with adenosine or an adenosine analogue (Fig. 2 shows a standard OMIT map, $F_o - F_o$, contoured at 3σ for the ligands in the ABS).

The ABS provides eight possible hydrogen-bond interactions between the protein and adenosine molecules. In five cases the enzyme acts as a donor (Asn14 $N^{\delta2}\cdots$N1, Gly64 N$\cdots$O2′, Ala65 N$\cdots$N3, Asn68 $N^{\delta2}\cdots$O3′ and Thr136 $O^{\gamma1}\cdots$N7) and in three it acts as an acceptor (Asp18 $O^{\delta1}\cdots$O2′, Asp18 $O^{\delta2}\cdots$O3′ and Asp302 $O^{\delta2}\cdots$O5′). The aspartic acid at position 18 is a highly conserved residue in these enzymes. It is not directly involved in catalysis, but the hydrogen bonds between the ribose group and the Asp18 side chain help to fix the adenosine moiety in the correct orientation favouring catalysis. The interaction is strong enough to change the original ribose conformation in adenosine, making it more flat and rigid, compatible with the O4′-*endo* sugar pucker conformation. Aspartic acid 302 is another highly conserved residue. It is important to keep the adenosine O5′ hydroxyl group appropriately oriented to receive the γ-phosphate from the ATP molecule and to

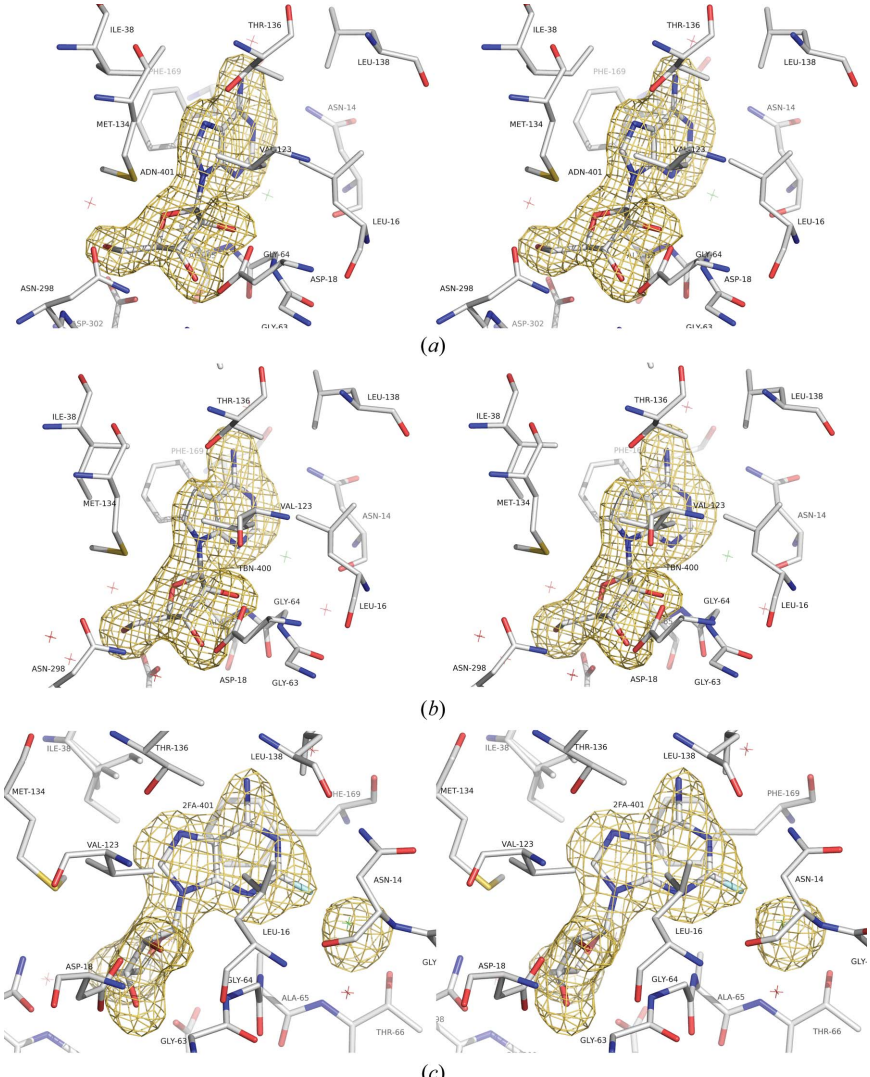

Figure 2
Stereoview of a standard OMIT map ($F_o - F_c$) at 3σ for ligands in the adenosine-binding site. (*a*) Adenosine. (*b*) Tubercidin. (*c*) 2-Fluoroadenosine; in this figure, the chloride ion is also shown in the OMIT map.

act as a proton acceptor during the reaction. Finally, it is of note that in the schistosome enzyme Asn14 forms hydrogen bonds to both N1 of the base and the side chain of Thr173. The consequence is to draw the loop from 172 to 175 closer to the base than in the human enzyme, where the latter interaction is lost owing to a substitution by a valine.

As observed in the human and *T. gondii* enzymes, SmAK has a chloride ion in the ABS. This ion is anchored by the positive terminus of the dipole associated with helix 3 and by direct interaction with the main-chain N atom of Asn14, the O^{γ} atom of Thr66 and water w1. In three of the ten structures described here the chloride ion also interacts with the main chain of Thr66.

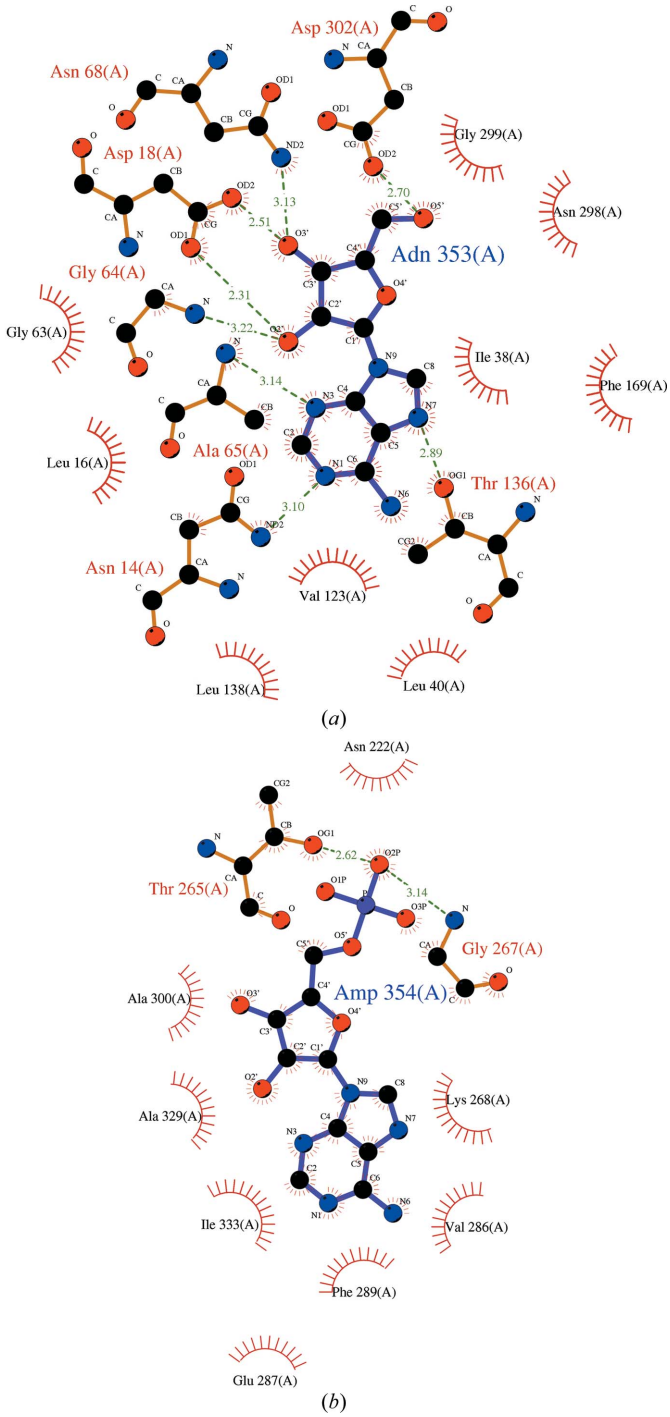

Figure 3
LIGPLOT diagrams (Wallace *et al.*, 1995) for the interactions of (*a*) adenosine and (*b*) AMP in their binding sites.

The base moiety of the adenosine is stacked between the side chains of Leu16 and Phe169, with other, mainly hydrophobic, contributions coming from Ile38, Gly63, Val123 and Leu138, as shown in Fig. 3. Only one water-mediated interaction was observed (Ado N6 with Phe169 O and with Asn172 $O^{\delta1}$). Water w370 (in SmAK), which interacts with N6 of the base, is conserved in the human and *T. gondii* structures [w416 in human AK (PDB entry 1bxu) and w1038 in *T. gondii* AK (PDB entry 1lik)] and mediates a water bridge between N6 and Phe169 O and Asn172 $O^{\delta1}$.

Tubercidin is a 7-deazaadenosine analogue and consequently does not form a hydrogen bond at this position to Thr136. However, an additional hydrogen bond is gained between Asn68 $N^{\delta2}$ and O3′ owing to a slightly different orientation of tubercidin within the active site. However, this interaction is also observed in the *B* subunit of the SmAK–Ado–AMP complex and we assume that the flexibility in the orientation of the adenosine moiety is correlated with the formation or disruption of this interaction.

We were only able to identify 2-fluoroadenosine bound to one of the two SmAK molecules present in the asymmetric unit (Fig. 2). The electron density indicates the presence of an additional atom at position 2 of the base which is compatible with a fluorine. The ligand shows the same interactions with the ABS as described previously for adenosine in the SmAK–Ado–AMP complex. The presence of the F atom at position 2, interacting with the chloride ion in the ABS, is the main difference compared with the remaining complexes described here. The crystallographic structure shows a short distance of 2.4 Å between the two atoms. However, with atom coordinate errors of 0.3 and 0.33 Å, the standard error in this distance is 0.45 Å; it is therefore only 2σ shorter than a standard F$\cdots$Cl nonbonded contact. The estimated coordinate errors were calculated from the Cruickshank DPI values (Cruickshank, 1999) to be 0.33 and 0.30 Å for chloride and fluorine, respectively, using coordinate error of atom = DPI $\times$ $(B_{\rm atom}/B_{\rm average})^{1/2}$. Such a configuration may initially look prohibitive. However, both atoms are under the influence of the dipole of helix 3, which appears to stabilize the system. On the other hand, this short distance could explain the preference for adenosine over 2-fluoroadenosine as observed in the activity assays.

Docking has been used to investigate the structural basis for the selectivity demonstrated by a group of compounds assayed by el Kouni & Cha (1987). They described that all nine of the compounds tested were able to bind and to be converted to monophosphate analogues by human AK. Indeed, the docking procedure used here was capable of reproducing the binding of these compounds to the human enzyme without any rotamer changes to the active-site residues. The docking procedure was also able to suggest the structural basis for the selectivity of the *Schistosoma* enzyme. As observed by

el Kouni and Cha, SmAK is able to form complexes with the following molecules: 7-deazaadenosine, nebularine, 7,9-dideaza-7-thioadenosine, 2-fluoro-2-deoxyadenosine and 9-deazaadenosine. These molecules docked well into the active site without inducing any alterations to the active-site rotamers. On the other hand, the compound 1-methylformycin has been reported to be a weaker ligand for SmAK compared with the human enzyme. The docking approach shows that this ligand only fits well inside the active-site cavity when Ile38 changes its side-chain conformation. Indeed, the crystallographic structures presented here show four different rotamers for this residue, demonstrating the feasibility of this modest conformational change.

el Kouni *et al.* (1987) also demonstrated that SmAK was unable to bind and catalyze the conversion of sagivamycin, 3-deoxysagivamycin and toyocamycin to their respective monophosphates. This result was also reproduced using our docking procedures. Our results show that large substituents at position 7 of the purine ring cause steric clashes between these bulky groups and Ile38, even when considering this residue to be flexible.

3.2.2. ATP-binding site. The ATP-binding site was characterized by examining the interactions made by AMP and tubercidin in the SmAK–Ado–AMP and SmAK–tubercidin complexes. Fig. 4 shows the standard $F_o - F_c$ OMIT map contoured at 3σ for the ligands and Fig. 3 shows a *LIGPLOT* diagram for AMP in the ATP-binding site. The presence of tubercidin in the ATP-binding site is probably a consequence of the high concentration used in the cocrystallization experiments (2 m*M*). However, it presents significantly higher temperature factors (62.61 Å^2) in comparison with other ligands (Table 1) as a consequence of weaker contacts within the ATP-binding site. Indeed, tubercidin makes no direct hydrogen bonds with the ATP-binding-site residues, forming only one water-mediated contact with Thr265 and two further hydrogen bonds with water 391 involving the N3 and O2′ atoms of the ligand.

Analogous binding of adenosine to the ATP-binding site has been observed previously in human AK (PDB entry 1bx4). In this case, residue Gln289 makes two hydrogen bonds to N6 and N1 of the adenine moiety of adenosine. In SmAK this residue is replaced by aspartic acid (Asp291), the side chain of which points away from the ATP-binding site, and we assume that the residue Asp291 does not participate in this binding site. The lack of a specific interaction with the 6-amino group suggests that GTP could be utilized as a phosphate donor in the AK reaction, as observed in other AKs.

In the SmAK–Ado–AMP complex, the AMP occupies part of the ATP-binding site, forming five hydrogen-bond interactions (subunit *A*). Three of these are formed with water molecules and two with the main-chain amide of Gly267 and the O$^\gamma$ atom of Thr265. In subunit *B* the AMP forms only two hydrogen bonds.

One remarkable difference encountered in the ATP-binding site of SmAK in comparison with its human counterpart is the observation of two different conformations for

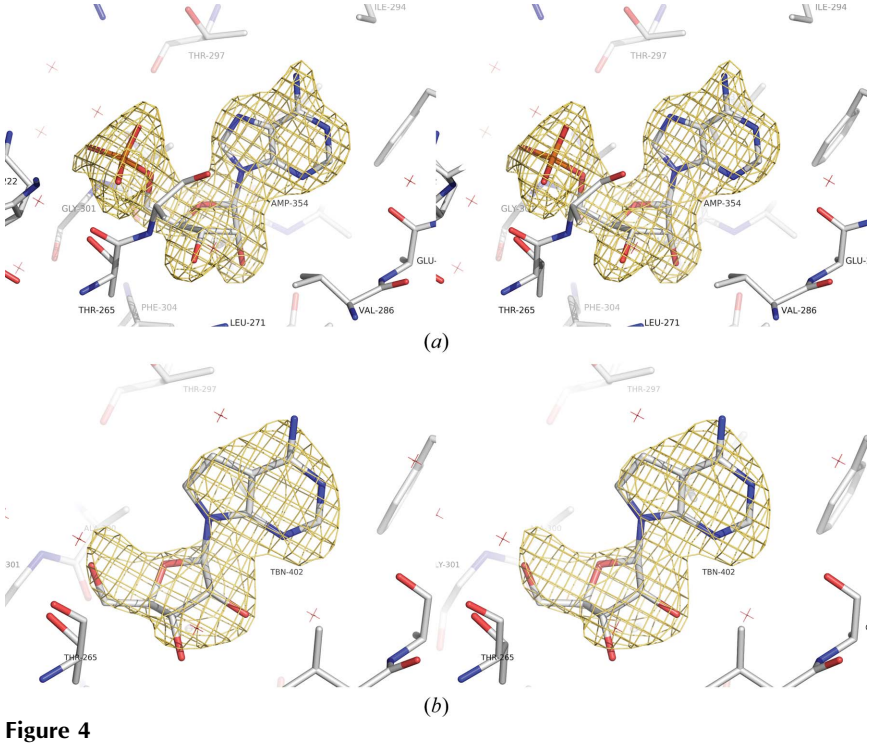

Figure 4
Stereoview of a standard OMIT map ($F_o - F_c$) at 3σ for AMP (*a*) and tubercidin (*b*) in the ATP-binding site (molecule *A*). The average *B* factor for tubercidin is very high (61.62 Å^2) as a result of very loose contacts within the ATP-binding site, leading to less well defined electron density.

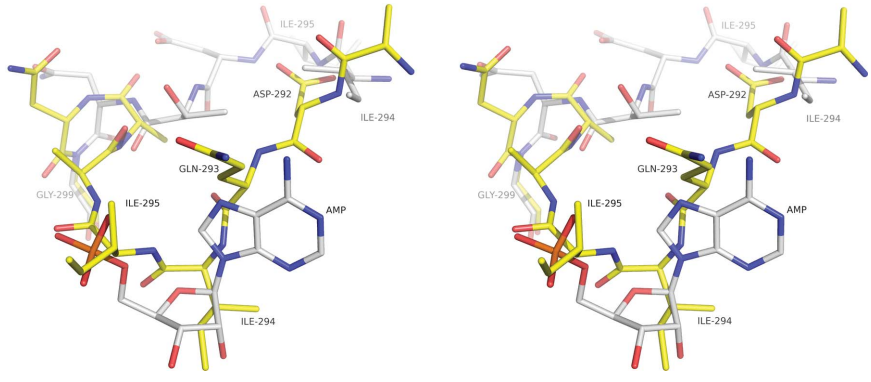

Figure 5
Superposed stereo images of the loop from 286 to 299 in the SmAK–AMP–adenosine complex (white) and the SmAK–adenosine complex (yellow; occluded loop structure). In the latter, residues 293–295 occupy the position of AMP observed in the former.

the loop spanning residues 286–299 (Figs. 5 and 6). We describe these conformations as occluded when the loop enters the ATP-binding pocket (as in SmAK–adenosine subunit *B*, SmAK–2-fluoroadenosine subunit *A* and SmAK–tubercidin subunit *B*) and open (the remaining structures). The occluded loop conformation has not been observed previously in other AKs. A further indicator of the great flexibility of this region is the absence of part of the loop in molecule *B* of SmAK–Ado–AMP (open conformation) and SmAK–tubercidin (occluded conformation).

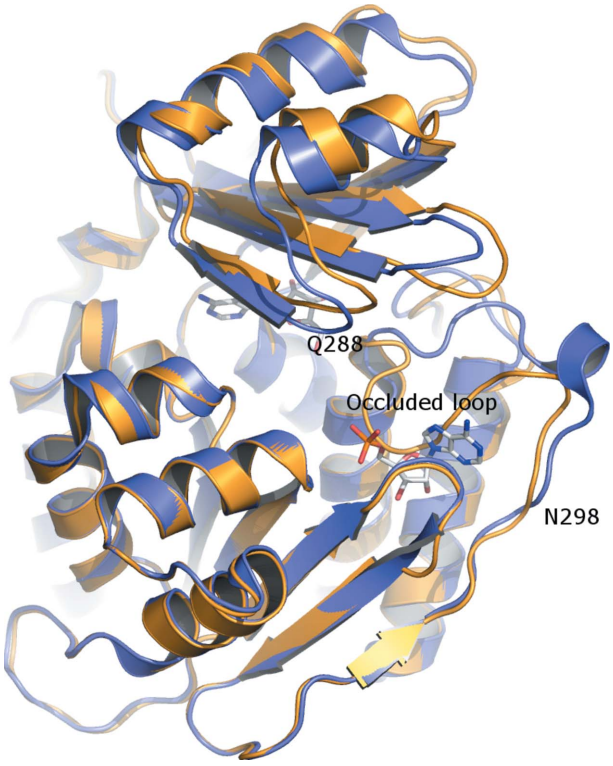

Figure 6
Superposition of SmAK–AMP–adenosine (blue; AMP molecule in white) and SmAK–adenosine (orange) in ribbon representation showing the different conformations for the 286–299 loop and also for the lid domain.

In the occluded conformation, residues Gln293, Ile294 and Ile295 occupy part of the ATP-binding site (Fig. 5). The aliphatic side chain of Ile294 points into the hydrophobic pocket created by residues Leu271, Val286, Phe289, Phe304 and Val326. The binding site of the ribose moiety of AMP is occupied in part by residue Ile294 and, finally, the position of the α-phosphate of AMP is occupied by the main chain and side chain of Ile295 (Fig. 5). We speculate that this loop in SmAK may exist in three different conformations, occluded, closed as observed in the *T. gondii* structure (PDB entry 1lio; Schumacher *et al.*, 2000) and open; the occluded conformation must obviously undergo a conformational change in order to bind ATP (Fig. 6).

3.3. Activity assays and the structural basis for differential nucleoside-analogue incorporation

Sequence and structural comparisons between *Schistosoma* and human AK reveals that the ABS possesses five potentially important differences: Ile38Gln, Ala65Ser, Val123Cys, Met134Leu and Thr136Ala (the residues observed in the *Schistosoma* sequence are shown prior to the residue number; see Fig. 7).

As mentioned above, the side chain of Ile38 is present in four different conformations in the various SmAK structures described here, acting as a filter which determines whether or not substituent groups at base position N7 are tolerated. In general terms, the side chain of Ile38 together with Thr136 limits the size of tolerable substituents at N7, preventing the binding of nucleosides with bulky groups at this position. Additionally, the presence of Thr136 provides extra hydrogen-bonding potential within the ABS, acting synergistically with Ile38 in the selection of permitted nucleosides. Indeed, the presence of Thr136 results in the formation of a hydrogen bond between its $O^{\gamma 1}$ atom and the N atom at position 7 of the base. This interaction is also observed in AK from *T. gondii*.

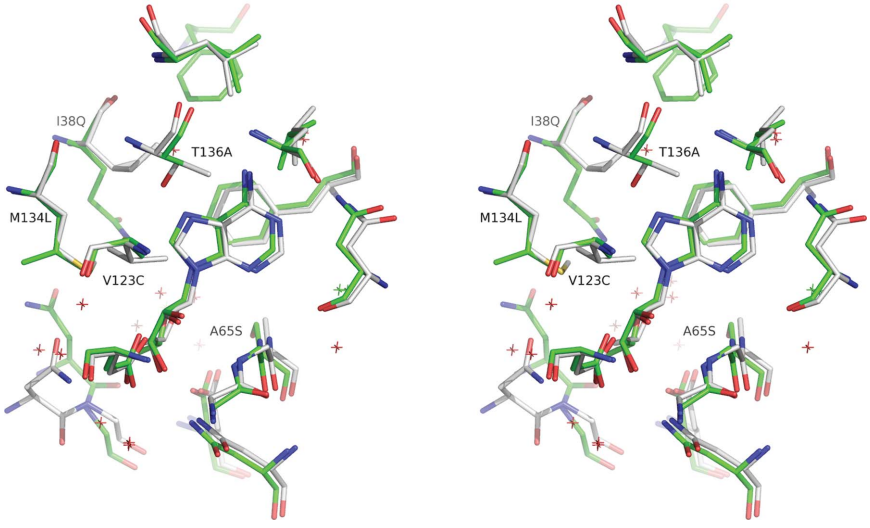

Figure 7
Stereo image of the adenosine-binding site of molecule *A* of the SmAK–AMP–adenosine ternary complex. The labels refer to the substitutions found in SmAK (white) in comparison with its human counterpart (green).

These structural features are probably responsible for the observed differences in the incorporation of nucleoside analogues into the nucleoside pool by schistosomes (el Kouni & Cha, 1987). These authors demonstrated the inability of schistosomes to phosphorylate nucleoside analogues with bulky groups at N7, such as sangivamycin, 3′-deoxysangivamycin and 1-methylformicin. Nevertheless, the parasite is able to use AK to phosphorylate closely related analogues such as formycin A and toyocamycin to their respective nucleotides. However, the conversion of toyocamycin (which possesses a methyl group on N7) to

toyocamycin nucleotides occurs in only small amounts, which is in agreement with an intolerance for bulky N7 substituents. On the other hand, tubercidin and nebularine (which have no N7 substituent) are readily incorporated into the nucleotide pool. In the case of the human enzyme, 1-methyformicin, toyocamycin, sangivamicin and 3′-deoxysangivamycin, all of which possess N7 substituents, can all readily be used as substrates (el Kouni & Cha, 1987). The crystal structures reported here strongly suggest that the principal bases of these differences are the Ile38Gln and Thr136Ala substitutions within the active site.

In the human enzyme the O^{γ} atom of Ser65 makes a strong hydrogen bond to $O^{\delta1}$ of Asp300, which itself interacts with O5′ of the sugar moiety *via* its $O^{\delta2}$ atom. In SmAK the presence of alanine in this position abolishes the interaction with the aspartic acid, rendering it less locked in by hydrogen bonds and conceivably more flexible. This in turn may have a knock-on effect on its interaction with O5′ of the ribose. The remaining two differences (Val123Cys and Met134Leu) do not significantly alter the ABS, as they maintain the overall hydrophobic environment.

It was of interest to determine the relative efficiency with which the schistosome enzyme is able to phosphorylate the substrates investigated in the present study *in vitro*. The values obtained for the specific activities were 59 ± 2 n*M* min^{-1} mg^{-1} for adenosine, 87 ± 2 n*M* min^{-1} mg^{-1} for tubercidin and 31 ± 1 n*M* min^{-1} mg^{-1} for 2-fluoroadenosine (2FA). The activity for tubercidin is 47% higher and that for 2FA is 52% lower when compared with adenosine. The lower activity for 2FA could be explained in terms of steric conflict between the fluoride moiety of 2FA and the chloride ion anchored deeply in the ABS; however, this is obviously not prohibitive for catalysis. Indeed, it has been known for many years that the 2FA analogue can be used as a substrate (Senft & Crabtree, 1977). Intact *S. mansoni* worms were able to metabolize 30% of the 2FA provided as substrate when incubated for 2 h in the presence of both 100 µ*M* adenosine and 2-fluoroadenosine. The phosphorylated products produced by AK were metabolized to 2-fluoro-ATP by the combined action of adenylate kinase and nucleoside diphosphate kinase. However, the product of the AK reaction, 2-fluoro-AMP (Long & Parker, 2006) is not a substrate for human erythrocyte adenylate kinase, indicating important differences in the metabolism of the nucleoside monophosphate analogues between the two species.

The higher activity for tubercidin compared with adenosine is an unexpected discovery since it appears to be in disagreement with the studies of Dovey *et al.* (1985). These authors showed that the incorporation of tubercidin and formycin A in schistosomules occurs at rates of one-tenth and one-fiftieth of the rate observed for adenosine. These analogues were also converted into their corresponding monophosphates, diphosphates and triphosphates. However, direct comparison between *in vivo* and *in vitro* studies is complex. The lower rates of incorporation could arise from several factors such as differences in the transport efficiency of the nucleoside analogues.

With respect to our *in vitro* observations, one possible explanation for the higher activity observed for tubercidin is the absence of a hydrogen bond between Thr136 and the base. A preference for tubercidin over adenosine has also been observed in sarcoma 180 human tumour cells (Divekar & Hakala, 1971), human tumour type H.Ep.No2 (Schnebli *et al.*, 1967) and in *Leishmania donovani* (Datta *et al.*, 1987).

The measured parameters for the ATP kinetics of SmAK are $K_m = 90.06 \pm 7.60$ µ*M*, $k_{cat} = 57.72 \pm 1.72$ s^{-1} and $k_{cat}/K_m = 0.64$ µM^{-1} s^{-1}. The value of the K_m for ATP of SmAK is slightly higher than that of the human liver AK enzyme (73 µ*M*; Yamada *et al.*, 1981) and could be attributed to the difference Asp291/Gln289, as previously described, that points towards the ATP-binding site.

Dovey *et al.* (1985) have previously emphasized the unusual substrate specificity of the *S. mansoni* enzyme, which recognizes tubercidin and formycin A but not adenine arabinoside or 9-deazaadenosine, making AK an important potential target for comparative host–parasite studies aimed at developing rational chemotherapy. However, as a warning note, it should be borne in mind that adenosine kinase is only found at low levels in *S. mansoni* extracts and its role in the adenosine-salvage pathway needs to be further clarified given the existence of an alternative route for producing AMP from adenosine *via* inosine, hypoxanthine and IMP. Nevertheless, the structures of SmAK reported here provide a structural explanation for the differential adenosine-analogue incorporation described by el Kouni a quarter of a century ago, which appears to be a consequence of the presence of residues Ile38 and Thr136 in the adenosine-binding site, which block the entrance of nucleosides with bulky N7 substituents. The modifications observed within this cavity suggest that there could be scope for elaborating specific inhibitors in the future.

The structural biology of schistosomes is an open field of research, with only 13 different protein structures available in the PDB. SmAK is the third enzyme to be described from the purine-salvage pathway of *S. mansoni*; the first was purine nucleoside phosphorylase (Pereira *et al.*, 2005; Pereira, Berdini *et al.*, 2010; Pereira, Rezende *et al.*, 2010) and the second was adenylate kinase (Marques *et al.*, 2012). Given the importance of the purine-salvage pathway for parasite metabolism, we are currently undertaking a systematic approach to investigating the structural biology and kinetics of the enzymes involved. It is expected that this knowledge will provide a more rational basis for target selection in the future. Specifically, this knowledge is necessary in order to understand the ways in which the parasite could be selectively starved of resources, which could be used to develop new drugs and/or vaccines against this second most important human parasite.

4. Conclusion

We have described a possible structural explanation for the different incorporation of adenosine analogues in *S. mansoni* compared with the human host, clarifying data reported a quarter of a century ago. We suggest this to be a consequence

of steric hindrance caused by the side chains of Ile38 and Thr136 in the adenosine-binding site of adenosine kinase, which restrict the binding of nucleosides with bulky N7 substituents. Nevertheless, there appears to be considerable flexibility within the binding cavities of the schistosome enzyme, which occurs at several levels. This is emphasized by the set of structures described here, in which structural plasticity is evident on comparing the different complexes reported and also from subunit to subunit within the asymmetric unit. Variation in the side-chain rotamers of Ile38 in the adenosine-binding site gives some degree of plasticity to the site, allowing many adenosine anologues to bind whilst remaining restrictive in terms of N7 substituents. On the other hand, previously unobserved flexibility within the ATP-binding-site loop 286–299 shows that this can be sterically occluded in the absence of ATP. Whilst the structural differences between the schistosome and human enzymes described here give hope for the potential development of specific inhibitors, target flexibility will continue to be a challenge for its effective implementation.

We gratefully acknowledge FAPESP fellowship support to LR and HMP. This work was financed by FAPESP and CNPq.

References

Adams, P. D., Grosse-Kunstleve, R. W., Hung, L.-W., Ioerger, T. R., McCoy, A. J., Moriarty, N. W., Read, R. J., Sacchettini, J. C., Sauter, N. K. & Terwilliger, T. C. (2002). *Acta Cryst.* D**58**, 1948–1954.

Battye, T. G. G., Kontogiannis, L., Johnson, O., Powell, H. R. & Leslie, A. G. W. (2011). *Acta Cryst.* D**67**, 271–281.

Carret, C., Delbecq, S., Labesse, G., Carcy, B., Precigout, E., Moubri, K., Schetters, T. P. & Gorenflot, A. (1999). *Eur. J. Biochem.* **265**, 1015–1021.

Cassera, M. B., Ho, M.-C., Merino, E. F., Burgos, E. S., Rinaldo-Matthis, A., Almo, S. C. & Schramm, V. L. (2011). *Biochemistry*, **50**, 1885–1893.

Chen, V. B., Arendall, W. B., Headd, J. J., Keedy, D. A., Immormino, R. M., Kapral, G. J., Murray, L. W., Richardson, J. S. & Richardson, D. C. (2010). *Acta Cryst.* D**66**, 12–21.

Cook, W. J., DeLucas, L. J. & Chattopadhyay, D. (2000). *Protein Sci.* **9**, 704–712.

Crabtree, G. W. & Senft, A. W. (1974). *Biochem. Pharmacol.* **23**, 649–660.

Cruickshank, D. W. J. (1999). *Acta Cryst.* D**55**, 583–601.

Datta, A. K., Bhaumik, D. & Chatterjee, R. (1987). *J. Biol. Chem.* **262**, 5515–5521.

Divekar, A. Y. & Hakala, M. T. (1971). *Mol. Pharmacol.* **7**, 663–673.

Dovey, H. F., McKerrow, J. H. & Wang, C. C. (1984). *Mol. Biochem. Parasitol.* **11**, 157–167.

Dovey, H. F., McKerrow, J. H. & Wang, C. C. (1985). *Mol. Biochem. Parasitol.* **16**, 185–198.

Emsley, P., Lohkamp, B., Scott, W. G. & Cowtan, K. (2010). *Acta Cryst.* D**66**, 486–501.

Hutchinson, E. G. & Thornton, J. M. (1996). *Protein Sci.* **5**, 212–220.

Kabsch, W. (2010). *Acta Cryst.* D**66**, 125–132.

el Kouni, M. H. (1991). *Biochem. Pharmacol.* **41**, 815–820.

el Kouni, M. H. & Cha, S. (1987). *Biochem. Pharmacol.* **36**, 1099–1106.

el Kouni, M. H., Messier, N. J. & Cha, S. (1987). *Biochem. Pharmacol.* **36**, 3815–3821.

Kuettel, S., Greenwald, J., Kostrewa, D., Ahmed, S., Scapozza, L. & Perozzo, R. (2011). *PLoS Negl. Trop. Dis.* **5**, e1164.

Lazarowski, E. R., Homolya, L., Boucher, R. C. & Harden, T. K. (1997). *J. Biol. Chem.* **272**, 20402–20407.

Long, M. C. & Parker, W. B. (2006). *Biochem. Pharmacol.* **71**, 1671–1682.

Marques, I. A., Romanello, L., Demarco, R. & Pereira, H. D. (2012). *Mol. Biochem. Parasitol.* **185**, 157–160.

Mathews, I. I., Erion, M. D. & Ealick, S. E. (1998). *Biochemistry*, **37**, 15607–15620.

McCoy, A. J. (2007). *Acta Cryst.* D**63**, 32–41.

Miech, F. P., Senft, A. W. & Senft, D. G. (1975). *Biochem. Pharmacol.* **24**, 407–411.

Miller, R. L., Adamczyk, D. L., Miller, W. H., Koszalka, G. W., Rideout, J. L., Beacham, L. M. III, Chao, E. Y., Haggerty, J. J., Krenitsky, T. A. & Elion, G. B. (1979). *J. Biol. Chem.* **254**, 2346–2352.

Pereira, H. M., Berdini, V., Ferri, M. R., Cleasby, A. & Garratt, R. C. (2010). *Acta Trop.* **114**, 97–102.

Pereira, H. D., Franco, G. R., Cleasby, A. & Garratt, R. C. (2005). *J. Mol. Biol.* **353**, 584–599.

Pereira, H. M., Rezende, M. M., Castilho, M. S., Oliva, G. & Garratt, R. C. (2010). *Acta Cryst.* D**66**, 73–79.

Schnebli, H. P., Hill, D. L. & Bennett, L. L. (1967). *J. Biol. Chem.* **242**, 1997–2004.

Schumacher, M. A., Scott, D. M., Mathews, I. I., Ealick, S. E., Roos, D. S., Ullman, B. & Brennan, R. G. (2000). *J. Mol. Biol.* **298**, 875–893.

Seeliger, D. & de Groot, B. L. (2010). *J. Comput. Aided Mol. Des.* **24**, 417–422.

Senft, A. W. & Crabtree, G. W. (1977). *Biochem. Pharmacol.* **26**, 1847–1855.

Senft, A. W. & Crabtree, G. W. (1983). *Pharmacol. Ther.* **20**, 341–356.

Senft, A. W., Crabtree, G. W., Agarwal, K. C., Scholar, E. M., Agarwal, R. P. & Parks, R. E. (1973). *Biochem. Pharmacol.* **22**, 449–458.

Senft, A. W., Miech, R. P., Brown, P. R. & Senft, D. G. (1972). *Int. J. Parasitol.* **2**, 249–260.

Senft, A. W., Senft, D. G. & Miech, R. P. (1973). *Biochem. Pharmacol.* **22**, 437–447.

Stegman, R. J., Senft, A. W., Brown, P. R. & Parks, R. E. (1973). *Biochem. Pharmacol.* **22**, 459–468.

Stein, N. (2008). *J. Appl. Cryst.* **41**, 641–643.

Trott, O. & Olson, A. J. (2010). *J. Comput. Chem.* **31**, 455–461.

Wallace, A. C., Laskowski, R. A. & Thornton, J. M. (1995). *Protein Eng.* **8**, 127–134.

Winn, M. D. *et al.* (2011). *Acta Cryst.* D**67**, 235–242.

World Health Organization (2005). *Report on Schistosomiasis.* Geneva: World Health Organization. http://www.who.int/entity/tdr/publications/documents/swg_schisto.pdf.

Yamada, Y., Goto, H. & Ogasawara, N. (1981). *Biochim. Biophys. Acta*, **660**, 36–43.

Zhang, Y., Dougherty, M., Downs, D. M. & Ealick, S. E. (2004). *Structure*, **12**, 1809–1821.

Zhang, Y., el Kouni, M. H. & Ealick, S. E. (2006). *Acta Cryst.* D**62**, 140–145.